

# PCCP

Accepted Manuscript



This is an *Accepted Manuscript*, which has been through the Royal Society of Chemistry peer review process and has been accepted for publication.

*Accepted Manuscripts* are published online shortly after acceptance, before technical editing, formatting and proof reading. Using this free service, authors can make their results available to the community, in citable form, before we publish the edited article. We will replace this *Accepted Manuscript* with the edited and formatted *Advance Article* as soon as it is available.

You can find more information about *Accepted Manuscripts* in the [Information for Authors](#).

Please note that technical editing may introduce minor changes to the text and/or graphics, which may alter content. The journal's standard [Terms & Conditions](#) and the [Ethical guidelines](#) still apply. In no event shall the Royal Society of Chemistry be held responsible for any errors or omissions in this *Accepted Manuscript* or any consequences arising from the use of any information it contains.

# The Low Frequency Motions of Solvated Mn(II) and Ni(II) Ions and their Halide Complexes

Vinay Sharma,<sup>a</sup> Fabian Böhm,<sup>a</sup> Gerhard Schwaab<sup>\*a</sup> and Martina Havenith<sup>a</sup>

Received Xth XXXXXXXXXXXX 20XX, Accepted Xth XXXXXXXXXXXX 20XX

First published on the web Xth XXXXXXXXXXXX 200X

DOI: 10.1039/b000000x

We have investigated the low frequency (30–350 cm<sup>-1</sup>) spectra of solvated MnCl<sub>2</sub>, MnBr<sub>2</sub>, NiCl<sub>2</sub>, and NiBr<sub>2</sub>. Using a chemical equilibrium model in combination with principal component analysis, we were able to dissect the spectra into molar extinction coefficients due to the solvated ions and – for MnCl<sub>2</sub>, MnBr<sub>2</sub>, and NiCl<sub>2</sub>– to extract information on the ion pair spectra. The deduced anion spectra (calculated as MnCl<sub>2</sub>-MnBr<sub>2</sub> and NiCl<sub>2</sub>-NiBr<sub>2</sub>) are very similar and nearly identical to the anion spectra observed for LaCl<sub>3</sub>-LaBr<sub>3</sub>. The differences between the cationic contributions MnCl<sub>2</sub>-NiCl<sub>2</sub> and MnBr<sub>2</sub>-NiBr<sub>2</sub> indicate, that the solvated cation spectra can be understood in terms of distinct resonances of the octahedrally solvated cation complex that are red-shifted for Mn<sup>2+</sup> compared to Ni<sup>2+</sup>. The description of the full extinction spectra requires the introduction of an additional resonance at a center frequency around 130 cm<sup>-1</sup> that we tentatively assign to hydration water. Cooperative effects are small and are reflected in a change in the band intensity. However, the center frequencies of the observed modes remain unchanged when exchanging the counter ion. Analysis of the ion pair extinction spectra support contact ion pair formation for MnBr<sub>2</sub> and NiCl<sub>2</sub> and MnCl<sub>2</sub>.

## 1 Introduction

The structure and dynamics of solvated ions is a central topic in chemistry and is of relevance for atmospheric science<sup>1</sup>, industrial applications<sup>2</sup> and biochemical processes.<sup>3,4</sup> At intermediate to high electrolyte concentrations ion pairing<sup>5,6</sup> hampers in many cases a detailed microscopic understanding of the solvent mediated interaction of cations, anions, and their cosolvents. Although a variety of experimental and theoretical methods has been developed over the years,<sup>3,7–12</sup> a generalized picture remains elusive. Distinct combinations of cations (e.g. Li<sup>+</sup>, Na<sup>+</sup>, Cs<sup>+</sup>, Mg<sup>2+</sup>, Gd<sup>3+</sup>), with counter anions (e.g. Cl<sup>-</sup>, Br<sup>-</sup>, SO<sub>4</sub><sup>2-</sup>, NO<sub>3</sub><sup>-</sup>) affect the hydration dynamics in a more complex way than initially assumed.<sup>7,8,10</sup> While some of these ions show negligible effects on the hydrogen bond dynamics<sup>13</sup> others are well known to show significant ion-complexation<sup>14</sup>. Therefore, it is important to explore their hydrogen bond dynamics at a molecular level.

Structure and dynamics of ionic solvation shells are also key factors when determining the physico-chemical properties of an electrolyte solution. A substantial amount of studies has been carried out to understand the different aspects of hydration for alkali and earth alkali halides.<sup>7,9–12</sup> Various experimental techniques have demonstrated that these ions affect the hydrogen bond network locally,<sup>12,13,15–17</sup> at variance to the older concept of a structure making (kosmotropic) or structure breaking (chaotropic) global influence.<sup>10</sup> Nowadays a picture emerges where the mutual electrostatic and dispersion

interactions between anions, cations, and surrounding water molecules govern the average hydration mechanism.<sup>13,15,18</sup>

Compared to the main group metals, the hydration of transition metal ions shows an increased variability.<sup>11,19,20</sup> Here, additional factors come into play such as ligand-field stabilization,<sup>21,22</sup> higher mass and a different kind of ligand-exchange kinetics compared to alkali and alkaline earth metal ions.<sup>8</sup> In addition to this, some d-transition metal ions show significant ion-complexation with counter anions while for other cases this tendency is negligible.<sup>14,19</sup> In the following we will focus on the transition metal ions Ni<sup>2+</sup> and Mn<sup>2+</sup>. In dilute solution, both show six-fold coordination with octahedral symmetry.<sup>7,11</sup> The increased ligand field stabilization of the Ni<sup>2+</sup> ion compared to Mn<sup>2+</sup> results in an increased binding energy and a smaller metal-oxygen distance in aqueous solution as confirmed both by theory<sup>21</sup> and experiment.<sup>7</sup> The effect is large enough to change the water exchange mechanism from I<sub>a</sub> (strong bond formation between entering ligand and complex) to I<sub>d</sub> (strong bond formation) for Mn<sup>2+</sup> and Ni<sup>2+</sup>, respectively,<sup>8</sup> and to influence the center frequency of the  $\tilde{\nu}_1$  Raman band of the solvated ion from 358 to 390 cm<sup>-1</sup>.<sup>23</sup>

The solvation structure and dynamics of NiCl<sub>2</sub> and NiBr<sub>2</sub> has been investigated by a variety of experimental methods, such as transference number measurements,<sup>24</sup> NMR,<sup>25,26</sup> neutron<sup>20,27</sup> and x-ray scattering<sup>28,29</sup>, extended X-ray absorption fine structure (EXAFS),<sup>30,31</sup> x-ray absorption near-edge structure (XANES),<sup>32</sup> and Raman spectroscopy<sup>23,33</sup> as well as molecular dynamics (MD), quantum mechanics/molecular

mechanical (QM/MM) MD, DFT, and Car-Parinello molecular dynamics (CPMD) simulations.<sup>31,34,35</sup> Less is known for  $\text{Mn}^{2+}$ .<sup>36–40</sup> While for low concentrations, there is general agreement on the structure of solvated  $\text{Ni}^{2+}$  and  $\text{Mn}^{2+}$ , the tendency to form complexes of manganese and nickel ions with counter halide anions is still not well understood.<sup>20,27–29,31,37</sup>

Here, we report a far-infrared (FIR) spectroscopic investigation of the hydration dynamics of  $\text{Mn}^{2+}$  and  $\text{Ni}^{2+}$  with  $\text{Cl}^-$  and  $\text{Br}^-$  as counter anions in aqueous solution using a broadband commercial Bruker Fourier transform infrared (FTIR) instrument.<sup>15,17</sup> Recently we demonstrated that this frequency range allows to probe the solvation dynamics of various solute molecules (e.g. proteins<sup>41</sup>, sugars,<sup>42,43</sup> and ionic salts<sup>15,17,44</sup>). A non-linear concentration dependence of the increase in absorption upon addition of salts was taken as evidence for ion complex formation.<sup>44</sup> When we record spectra in the frequency range 30–350  $\text{cm}^{-1}$ , we find that in case of ion complexation the observed spectrum changes. At low concentrations we find clearly separated solvated cation and anion resonances whereas at high concentration the spectrum is dominated by ion-complex bands. For monovalent, divalent and lanthanide halide salts we were able to assign low energy vibrational resonances of distinct ions with their hydration shell.<sup>17,44</sup> In the following, we will show that this spectroscopic technique is also useful to dissect the observed extinction spectra not only into modes of the individual anions and cations but also to estimate the combined effect of anions and cations on the solvation water spectrum. We will also deduce information on the specific nature (solvent shared versus contact ion pair) of ion complexes forming in concentrated electrolyte solutions.

## 2 Materials and Methods

### 2.1 Materials

Both manganese and nickel halide salts were purchased from commercial chemical providers (Sigma Aldrich, ABCR Chemicals and Alfa Aesar) with a purity of > 99 % for  $\text{MnCl}_2$ ,  $\text{NiCl}_2$ ,  $\text{NiBr}_2$ , and > 98 % for  $\text{MnBr}_2$ . For each concentration of the molar concentration series in the range 0.5–4 M or up to the solubility limit the weighed out amount of salt was dissolved in HPLC grade ultra pure water. The density of each electrolyte concentration was determined using an Anton Paar DMA 58 density meter at  $20 \pm 0.2^\circ$ . The amount of hydrolysis was determined by pH measurements (see Table 1). All aqueous salt solutions show a decrease in pH with increasing molar concentration. While for  $\text{NiCl}_2$ ,  $\text{NiBr}_2$ , and  $\text{MnCl}_2$  even for the highest salt concentration of the hydrolysis product remains below 0.1 M,  $\text{MnBr}_2$  shows strong hydrolysis with increasing concentration.

salt concentration	$\text{NiCl}_2$	$\text{NiBr}_2$	$\text{MnCl}_2$	$\text{MnBr}_2$
0.5 M	4.4	6.5	6.1	2.7
2.0 M	–	4.2	–	2.0
3.0 M	–	–	–	0.4
4.0 M	3.3	–	1.3	-0.4

**Table 1** Measured pH values of the aqueous salt solutions under consideration for selected concentrations.

### 2.2 Far-Infrared Fourier Transform spectroscopy

Broadband FIR Fourier Transform absorption spectroscopic measurements were carried out using a Bruker Vertex 80 V FTIR spectrometer attached with a liquid helium cooled Si bolometer (Infrared Laboratories) as detector. For an extended description of the technique refer to Schmidt et. al.<sup>15</sup> We measured all electrolyte solutions in a concentrations range from 0.5 M to 4.0 M of  $\text{MnX}_2$  and  $\text{NiX}_2$ , X: Cl, Br). As sample holder served a commercial Bruker liquid cell with CVD grown diamond windows ( $500 \pm 100 \mu\text{m}$  thickness; Diamond Materials, GmbH). This guaranteed maximum transparency over a broad frequency range ( $50\text{--}370 \text{cm}^{-1}$ ). The liquid layer thickness was maintained using  $40 \pm 1 \mu\text{m}$  thick Kapton spacers. The exact spacing size was determined by recording the etalon fringes of the empty cell in a Fourier Transform spectrometer. We kept the liquid cell under continuous nitrogen gas purging and temperature controlled conditions ( $20 \pm 0.2^\circ$ ) in a closed sample compartment which was separated by polyethylene flaps from the rest of the evacuated spectrometer chamber. Each spectrum was recorded with  $2 \text{cm}^{-1}$  resolution and averaged over 384 scans.

The resulting total absorption coefficient of an electrolyte solution is given by:

$$\alpha_{\text{solution}}(\tilde{\nu}) = -\frac{1}{d} \log \left( \frac{I_{\text{solution}}(\tilde{\nu})}{I_{\text{bulk}}(\tilde{\nu})} \right) + \alpha_{\text{bulk}}(\tilde{\nu}) \quad (1)$$

with  $d$  being the measured layer thickness,  $\alpha_{\text{bulk}}$  the absorption coefficient of the bulk water reference and  $I_{\text{bulk}}$  and  $I_{\text{solution}}$  being the transmitted intensities of the reference and sample, respectively. The water spectrum  $\alpha_{\text{bulk}}(\tilde{\nu})$  for the temperature of  $20^\circ\text{C}$  was obtained as fit from temperature dependent bulk water measurements that were referenced to a temperature of  $25^\circ\text{C}$  and to the published data of Bertie and Lan.<sup>45</sup> The functional form is given by Equation (9) in the appendix.

In order to remove nonlinearities due to the dependency of the apparent molar volume of the electrolyte on salt concentration we determined the effective ionic absorption  $\alpha_{\text{ion}}^{\text{eff}}$  of the solvated ions according to

$$\alpha_{\text{ion}}^{\text{eff}} = \alpha_{\text{solution}} - \frac{c_w}{c_w^0} \alpha_{\text{bulk}}(\tilde{\nu}) \quad (2)$$

with  $c_w$  and  $c_w^0$  as concentrations of water in the solution as

obtained from density measurements and in bulk water at the same temperature, respectively.  $\alpha_{\text{ion}}^{\text{eff}}$  contains the contributions from the ions and ion-associates as well as any change in the water absorption induced by the solvated ions compared to bulk water.<sup>44</sup> For an ideal bi-component (cation(aq) + anion(aq)) electrolyte solution with negligible ion association  $\alpha_{\text{eff}}^{\text{ion}}$  is proportional to the salt concentration. Nonlinear changes will therefore be especially prominent in the molar effective ionic extinction ( $\epsilon_{\text{ion}}^{\text{eff}} = \frac{\alpha_{\text{ion}}^{\text{eff}}}{c_s}$ ) that is obtained by normalizing the effective ionic absorption to the molar salt concentration  $c_s$ . For the ideal electrolyte solution  $\epsilon_{\text{ion}}^{\text{eff}}$  is expected to be independent of solute concentration.

### 3 Experimental Results

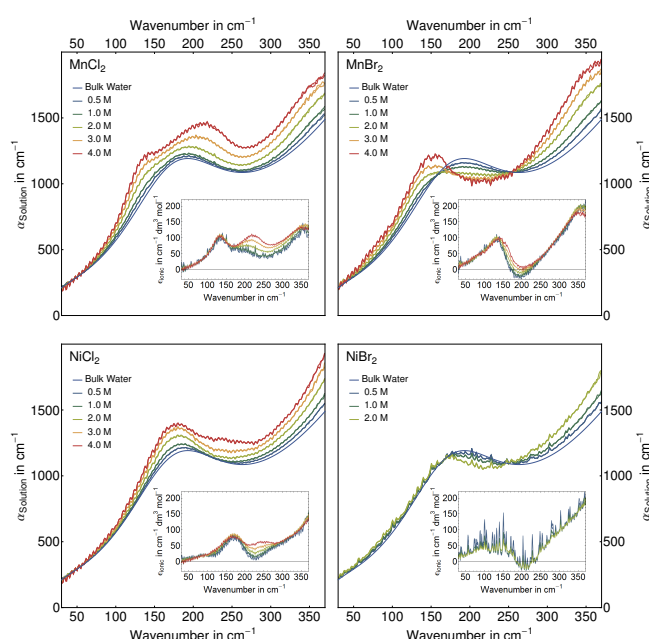


**Fig. 1** Absorption coefficient spectra of Mn(II) halides (top) and Ni(II) halides (bottom) as a function of concentration at  $20 \pm 0.2^\circ\text{C}$ . The insets show the corresponding effective ionic extinction spectra. The narrow lines prominent in the NiBr<sub>2</sub> spectra are due to different water vapor content in the sample spectrum with respect to the reference measurement. Note, that each measurement has been performed twice. In most cases the measurements agree within the linewidths displayed.

In Figure 1, we present the absorption coefficients at different salt concentrations (see materials and methods section) for both MnX<sub>2</sub> and NiX<sub>2</sub> (X: Cl, Br). For better visualization of the ion induced changes we also show the effective ionic extinction (see insets). All transition metal halides show distinct ionic resonances in the range from 30 to 350 cm<sup>-1</sup>

with a strong increase of absorption towards higher frequencies. The bromide spectra show two main resonances below 200 cm<sup>-1</sup>: one has been assigned before<sup>17</sup> to Br<sup>-</sup> at 90 cm<sup>-1</sup> and a second one to the cation with a center frequency of 140 and 150 cm<sup>-1</sup> for Mn<sup>2+</sup> and Ni<sup>2+</sup>, respectively. The cation absorption bands are also visible in the MnCl<sub>2</sub> (M: Mn, Ni) spectra. For both chlorides an additional peak is observed in the frequency range 200–250 cm<sup>-1</sup> which increases non-linearly with increasing concentration. In addition, we observe a partial negative effective ionic absorption for both NiBr<sub>2</sub> and MnBr<sub>2</sub> at low concentrations at the resonance (hindered translational motion<sup>46</sup>) of water at 200 cm<sup>-1</sup>. This provides a hint that the ions influence the water in their vicinity such that the hydration water in the solution shows an effective absorption that is either shifted in frequency or decreased in transition strength.

### 4 Spectrum Dissection and Discussion

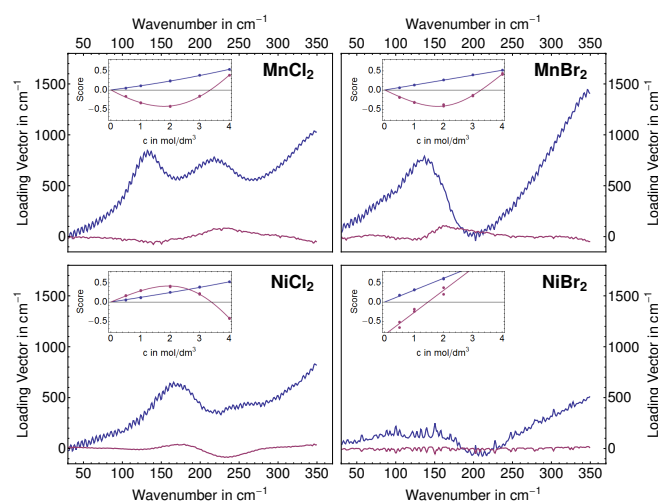


**Fig. 2** The primary (in blue) and secondary principal component (red) obtained in a singular value decomposition for the four salts investigated. The insets show the concentration dependency of the corresponding scores together with a global fit assuming ion pair formation (MnCl<sub>2</sub>, MnBr<sub>2</sub>, NiCl<sub>2</sub>). In the case of NiBr<sub>2</sub> the secondary component is linear and describes residual water vapor in the Fourier transform spectrometer. In all cases the primary and secondary components contain more than 95% of the information.

For further analysis we performed a principal component analysis of  $\alpha_{\text{ion}}^{\text{eff}}(\tilde{\nu})$  using

$$(\mathbf{S}, \mathbf{SV}, \mathbf{L}) = \text{SVD}(\mathbf{Data}) \quad (3)$$

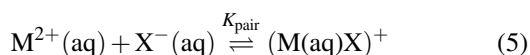
where SVD describes a singular value decomposition of the array Data that contains the individual measurements as row vectors.<sup>47</sup> The function returns three matrices: **S** contains the

scores of the principal components as row vectors,  $\mathbf{SV}$ , a diagonal matrix, the singular values, and  $\mathbf{L}$  the corresponding eigenvectors describing the data as column vectors. In the following, we will refer to a principal component as the product of eigenvector and its corresponding singular value.

Figure 2 shows the primary and secondary principal components for the four salts investigated. In all cases, the two components contain more than 95% of the information: the primary component ( $\approx 90\%$ ) describes the spectrum averaged over all concentrations, the secondary ( $\approx 5\%$ ) the changes relative to this average spectrum. The insets of Figure 2 show the concentration dependency of the scores. While the major component shows a mostly linear behavior, the secondary component is strongly non-linear with the exception of  $\text{NiBr}_2$ , where residual water vapor lines are visible in the spectra (see Figure 1). In a first step, we ascribe the non-linear behavior to ion pair formation which has been observed for many salts<sup>5</sup> (solvent separated: 2SIP, solvent shared: SIP, contact ion pair: CIP) based on the results of ultrasonic measurements and dielectric spectroscopy. Since two principal components are sufficient to describe the concentration dependence of our data, we will assume a single ion pair formation step. The underlying model has been described in detail in our previous paper on the solvation dynamics of lanthanides<sup>44</sup>. Briefly,  $\alpha_{\text{ion}}^{\text{eff}}(\tilde{\nu})$  is described as

$$\alpha_{\text{ion}}^{\text{eff}}(\tilde{\nu}) = c_s \epsilon_{\text{single}}^{\text{eff}}(\tilde{\nu}) + c_{\text{pair}}(c_s, K_{\text{pair}}) \epsilon_{\text{diff}}^{\text{eff}}(\tilde{\nu}), \quad (4)$$

i.e. a linear part due to total effective extinction  $\epsilon_{\text{single}}^{\text{eff}}(\tilde{\nu})$  of solvated anion and cation and a nonlinear part  $c_{\text{pair}}(c_s, K_{\text{pair}}) \epsilon_{\text{diff}}^{\text{eff}}(\tilde{\nu})$ .  $\epsilon_{\text{single}}^{\text{eff}}(\tilde{\nu}) = \epsilon_{\text{cation}} + \epsilon_{\text{anion}} - n_{\text{hydration}} \epsilon_{\text{bulk}}$  describes the sum of the cation and anion extinction coefficient minus a THz defect due to the effective number of hydration water molecules that show a spectrum different from the bulk water spectrum.  $\epsilon_{\text{diff}}^{\text{eff}}(\tilde{\nu})$  corresponds to the difference between the ion pair extinction and the anion and cation extinctions.<sup>44</sup> The non-linear concentration dependence of  $c_{\text{pair}}(c_s, K_{\text{pair}})$  of the equilibrium reaction



is determined by the association constant  $K_{\text{pair}}$  and the mean activity coefficients  $\gamma_{\text{anion}}$ ,  $\gamma_{\text{cation}}$ , and  $\gamma_{\text{pair}}$  of anion, cation and ion pair, respectively:

$$c_{\text{pair}}(c_s) = K_{\text{pair}} c_{\text{anion}} c_{\text{cation}} \frac{\gamma_{\text{anion}} \gamma_{\text{cation}}}{\gamma_{\text{pair}}}. \quad (6)$$

At this point, we have no *a priori* knowledge on the ion pair activity. However, to simplify Equation (6) and to reduce the number of fit parameters we may assume that the chemical structures of solvated ion-pair and solvated cation are similar yielding  $\gamma_{\text{pair}} \approx \gamma_{\text{cation}}$ . The comparison with the experimental data will show *a posteriori* if this assumption is valid.

The mean activity coefficients for manganese (II) chloride and bromide and nickel (II) chloride were taken from Goldberg et. al.<sup>48,49</sup>

The insets in Figure 2 show that the model is in good agreement with the concentration dependence of the scores when we use the fit parameters  $K_{\text{pair}}(\text{MnBr}_2)=0.059(6)$ ,  $K_{\text{pair}}(\text{MnCl}_2)=0.075(9)$ , and  $K_{\text{pair}}(\text{NiCl}_2)=0.048(6)$ . Removing the highest concentration measurement for  $\text{MnBr}_2$  changed  $K_{\text{pair}}(\text{MnBr}_2)$  to 0.122(14), indicating that the uncertainty in  $K_{\text{pair}}$  is underestimated by the statistical error. However, the single ion and ion pair spectra extracted with this method were only little effected. Therefore, we will use the full data set in the following discussion. Note that the described association constants have merely to be considered as fit parameters and are not directly comparable to the association constants obtained by other methods. The main reason is that we can not exclude a chain of reactions:  $\text{M}^{2+}(\text{aq}) + \text{X}^{-}(\text{aq}) \rightleftharpoons \text{SSIP} \rightleftharpoons \text{SIP} (\rightleftharpoons \text{CIP})$  where the solvated ions show a spectrum similar to the solvent separated ion pair. In such a case the fit would only return an effective value for  $K_{\text{pair}}$ . For  $\text{NiBr}_2$  we used the global fit shown in Figure 2 to remove the residual water vapor lines. Since the ion pair formation depends

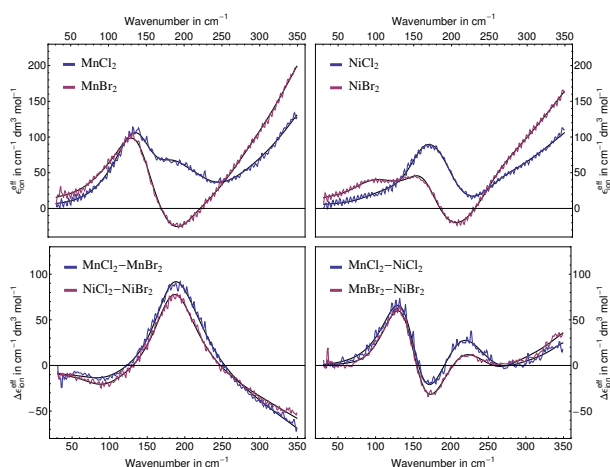


**Fig. 3** Top left: effective ionic extinctions for  $\text{MnCl}_2$  (blue) and  $\text{MnBr}_2$  (red). Top right: effective ionic extinction for  $\text{NiCl}_2$  (blue) and  $\text{NiBr}_2$  (red). Bottom left: difference in effective ionic extinctions emphasizing anion resonances showing  $\text{MnCl}_2$ – $\text{MnBr}_2$  in blue and  $\text{NiCl}_2$ – $\text{NiBr}_2$  in red. Bottom right: difference in effective ionic extinctions emphasizing cation resonances showing  $\text{MnCl}_2$ – $\text{NiCl}_2$  in blue and  $\text{MnBr}_2$ – $\text{NiBr}_2$  in red. The black lines display the predicted response from a global fit of all eight data sets as described in the text.

at least quadratically on concentration, the effective ion extinctions can be directly calculated from the slope of the score

functions  $s_i(c_s)$  evaluated at  $c_s = 0$ :

$$\epsilon_{\text{ion}}^{\text{eff}} = \sum_{i=1}^2 \left. \frac{ds_i}{dc_s} \right|_{c_s=0} \mathbf{V}_i \quad (7)$$

where  $\mathbf{V}_i$  denotes the  $i^{\text{th}}$  principal component and  $\frac{ds_i}{dc_s}$  the derivative of the score function belonging to principal component  $i$  with respect to the salt concentration. Figure 3 shows the effective ionic extinction spectra of the four measured salts as well as the differences of salts containing the same cation but different anions and vice versa. All ionic spectra  $\epsilon_{\text{ion}}^{\text{eff}}$  exhibit a high frequency wing extending to frequencies  $> 350 \text{ cm}^{-1}$  which is more prominent for the bromides compared to the chlorides. In the case of the nickel salts a prominent shoulder is visible around  $270\text{--}280 \text{ cm}^{-1}$ .  $\text{MnCl}_2$  displays two main peaks centered on  $130 \text{ cm}^{-1}$  and  $200 \text{ cm}^{-1}$ , respectively. For  $\text{NiCl}_2$  a broad resonance between  $140$  and  $220 \text{ cm}^{-1}$  is found. The ionic spectra of  $\text{MnBr}_2$  show a broad signature ranging from  $70\text{--}180 \text{ cm}^{-1}$ , while  $\text{NiBr}_2$  presents two distinct modes centered at  $90$  and  $150 \text{ cm}^{-1}$ . Both bromides display a frequency range of negative extinction centered around  $200 \text{ cm}^{-1}$ .

Concerning the difference spectra, the observed extinction differences for  $\text{MnCl}_2\text{--MnBr}_2$  and  $\text{NiCl}_2\text{--NiBr}_2$  show very similar behavior and resemble the difference spectrum of the La halides.<sup>44</sup> The differences of the cation spectra indicate the existence of at least two resonances per cation whose center frequencies are blue-shifted for  $\text{Ni}^{2+}$  with respect to  $\text{Mn}^{2+}$ . While the strongest resonance is observed to be independent of the anion, for  $\text{Mn}^{2+}$  the weaker resonance at higher frequency is sensitive to the counter ion.

In order to dissect the spectra some constraints on the number and range of fit parameters based on physical considerations and comparison to other measurements are required. In Sharma et al.<sup>44</sup> we used Lorentzian lineshapes to model the ionic resonances although we were aware that they do not show the proper limiting behavior when approaching zero frequency. The main reason for this approximation was that they allowed to fit the observed spectra with a minimum number of components including the low frequency region around  $30\text{--}50 \text{ cm}^{-1}$ . For low frequencies, we observe a positive contribution that we ascribe to the high frequency Debye relaxation mode observed in dielectric relaxation spectroscopy.<sup>50</sup> Such a Debye mode yields constant extinction up to infinite frequencies when converted to an absorption coefficient and neglect of inertial effects (see Nitzan,<sup>51</sup> chapter 8).

Here, we model the low frequency part of the spectrum as scaled relaxational part (mode 0 in Equation (9)) of water and use a slightly modified form of the damped harmonic oscillation

function as lineshape for the higher frequency modes:

$$\epsilon_{\text{DH}}(\tilde{\nu}) = \frac{a_0 w_0^2 \tilde{\nu}^2}{4\pi^3 \left[ \frac{\tilde{\nu}^2 w_0^2}{\pi^2} + \left( \tilde{\nu}_d^2 + \frac{w_0^2}{4\pi^2} - \tilde{\nu}^2 \right)^2 \right]} \quad (8)$$

where  $a_0$ ,  $w_0$ , and  $\tilde{\nu}_d$  are the amplitude, the width and the center frequency of the damped harmonic oscillator mode. The line shape corresponds to a Brownian harmonic oscillator with an unperturbed center frequency  $\tilde{\nu}_0 = \sqrt{\tilde{\nu}_d^2 + \left(\frac{w_0}{2\pi}\right)^2}$ . Note, that we have normalized  $\epsilon_{\text{DH}}$  to its value at  $\tilde{\nu}_0$  to minimize parameter cross correlations when performing a least squares fit.  $w_0$  is directly related to the decay time  $\tau$  of the autocorrelation  $\langle \mu(0)\mu(t) \rangle$  of the oscillator's dipole moment vector by  $\tau = \frac{1}{w_0 \times c}$  when  $w_0$  is given in wavenumber units and  $c = 3 \times 10^{10} \text{ cm/sec}$  is the speed of light (see Nitzan,<sup>51</sup> chapter 8). Thus we combine robustness of the fit and physically meaningful parameters.

To minimize the number of fit parameters we model the high frequency end of the spectra as scaled librational part of the water extinction (modes 2 and 3 in Equation (9), see also Table 3), respectively. A further reduction in model complexity is achieved by assuming that all eigen modes of the solvated ions in the solution couple to the same set of thermal bath states so that the corresponding dephasing time constants  $\tau$  and their corresponding damping factors are identical. In that case, the effective line width is proportional to the center frequency ( $w = \frac{w_0 \tilde{\nu}}{\pi} \approx \frac{w_0 \tilde{\nu}_0}{\pi}$ ) when  $\tilde{\nu}_0 \approx \tilde{\nu}_d$ .

#### 4.1 Ionic Contributions

As displayed in Figure 3, we find distinct resonances that are specific for the individual solvated ions. In addition, the effect of bromide on the libration band intensity seems to be increased compared to chloride. The cation difference spectra (Figure 3, Bottom row) can be well described by assigning three damped harmonic oscillator resonances to  $\text{Mn}^{2+}$  and two to  $\text{Ni}^{2+}$ . There is no sign of a different influence of both cations on the relaxational and librational part or any other part of the spectrum. The same holds for the anion differences where we find one resonance per anion in agreement with older data<sup>17,44</sup> with the exception of the high frequency component where we observe an increased influence of  $\text{Br}^-$  compared to  $\text{Cl}^-$ . However, an attempt to retrieve the observed ionic extinctions (Figure 3, top row) based solely on the spectral line shapes obtained from the difference spectra and additional low frequency and high frequency hydration water components failed. Figure 4 shows  $\text{NiCl}_2$  as an example: only when we include an additional resonance, all extinction spectra and their differences can be fit within our measurement error. Since this additional mode is not specific for any of the anions or cations, we tentatively assign it to hydration wa-

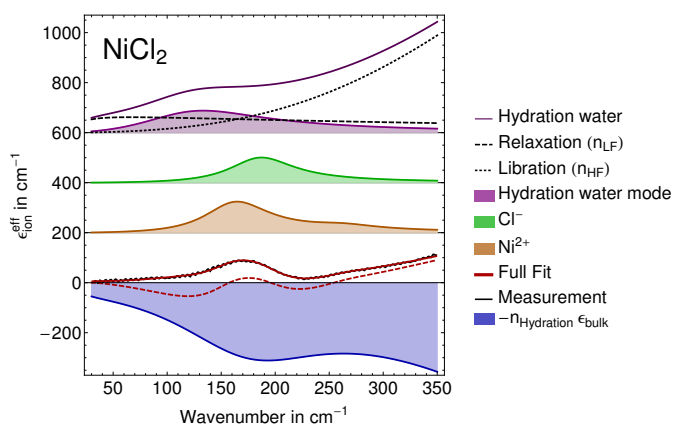


**Fig. 4** Individual contributions to the  $\text{NiCl}_2$  extinction spectrum (from top to bottom): hydration water (dark purple) as sum of scaled relaxational (dashed) and librational (dotted) bulk water modes and an additional damped harmonic oscillator mode (purple);  $\text{Cl}^-$  (aq) in green;  $\text{Ni}^{2+}$  in orange; the measured spectrum (black line) together with the best fit model function (in red). The negative blue line describes the THz defect ( $-n_{\text{hydration}}\epsilon_{\text{bulk}}$  due to hydration water. The dashed red line shows the fit model without the additional hydration water mode. While the anion and cation resonances are sufficient to reproduce the difference spectra (see Figure 3), this additional hydration water component is required to recover the measured spectra (black line).

ter. The similarity of the hydration water environment of the anions and cations investigated prevents a separation of anion and cation influences on the hydration water modes. The final, global fit of the eight spectra displayed in Figure 3 invoked 27 independent parameters (see Table 2. Figure 5 shows the contributions of the individual solvated ions and the effect of the different electrolytes on the surrounding solvation water obtained from the fit.

**4.1.0.1  $\text{Cl}^-$  and  $\text{Br}^-$  contributions:** The center frequencies of the unperturbed  $\text{Cl}^-$  and  $\text{Br}^-$  modes are located at  $188\text{ cm}^{-1}$  and  $94\text{ cm}^{-1}$  with  $\text{Mn}^{2+}$  and  $\text{Ni}^{2+}$  as counter cations, respectively. This assignment agrees very well with the band centers reported previously by us in case of monovalent, divalent and lanthanum halides.<sup>15,17,44</sup> The strong red shift in the resonance of  $\text{Br}^-$  compared to  $\text{Cl}^-$  can be explained by an increase in the anion mass in combination with a smaller confinement effect due to the larger ion radius of  $\text{Br}^-$ .<sup>7,52</sup> In addition, based on our model, we observed a small cooperative effect concerning the amplitudes but not the center frequencies of the observed resonances. Without support from theoretical calculations the origin of this experimental observation is unclear. On one side it could be due to a change in the strength of the transition dipole moment of the resonances due to different cross correlation terms for ions with different polarizabilities. On the other hand it could be a dy-

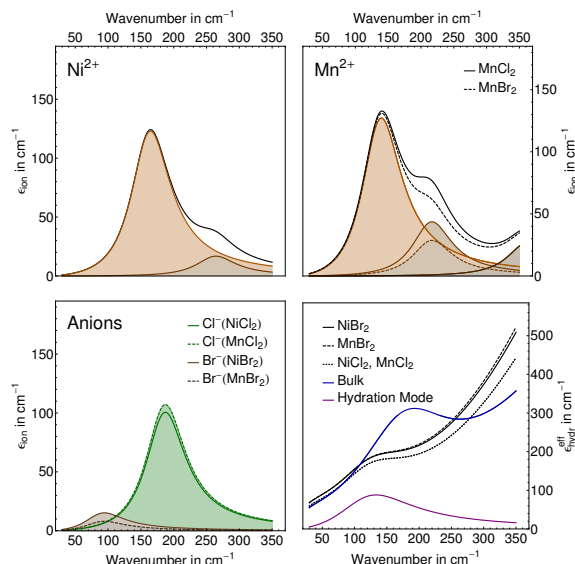


**Fig. 5** Top row: Solvated cation resonances for  $\text{Ni}^{2+}$  (left) and  $\text{Mn}^{2+}$  (right) and their individual spectral contributions. The total solvated cation spectrum is shown in black. Bottom row: solvated anion resonances for  $\text{Br}^-$  and  $\text{Cl}^-$  (left) and solvation water spectrum for the four different electrolytes investigated (right). The bulk water spectrum of 14.5 mole of bulk water obtained from the fit and the water mode observed for all electrolytes are shown as blue and purple lines, respectively. See text for a detailed discussion and Table 2 for a list of line parameters.

namic effect in the form that counter cations stabilize or destabilize the anionic solvation shell. In contrast to our previous paper<sup>44</sup> our refined model does not require a different number of water molecules affected by  $\text{Cl}^-$  compared to  $\text{Br}^-$ , but attributes the negative part in the high frequency anion difference spectrum to an increased interaction of the more polarizable  $\text{Br}^-$  with the water librational modes.

**4.1.0.2  $\text{Mn}^{2+}$  (aq) and  $\text{Ni}^{2+}$  (aq) contributions:** The solvated cation extinction spectra show some common characteristics: In both cases, we find two main resonances of similar peak intensity that are red-shifted for  $\text{Mn}^{2+}$  (aq) compared to  $\text{Ni}^{2+}$  (aq) (see Table 2). While  $\text{Mn}^{2+}$  (aq) ions show bands centered at  $\nu_0 = 140$  and  $217\text{ cm}^{-1}$  the  $\text{Ni}^{2+}$  (aq) resonances are located at  $165$  and  $265\text{ cm}^{-1}$ . For both cations, these resonances are assigned to normal modes of the cation with their octahedral hydration cage, similar to those observed in  $\text{MgCl}_2$ .<sup>17</sup> In contrast to  $\text{Ni}^{2+}$ ,  $\text{Mn}^{2+}$  (aq) shows an additional mode at  $362\text{ cm}^{-1}$ . It is interesting to note that this is close to the center frequency of  $358 \pm 5\text{ cm}^{-1}$  for the  $\nu_1$   $\text{Mn-OH}_2$  Raman stretching bands observed by Kanno et al.<sup>23</sup> for  $\text{MnCl}_2$ .

Funkner et al. assigned the  $\text{Mg}^{2+}$  mode observed around  $180\text{--}190\text{ cm}^{-1}$  to the motion of the  $\text{H}_2\text{O-Mg}^{2+}\text{-H}_2\text{O}$  inner axis moieties against the four water molecules in the plane

perpendicular to this axis in an octahedrally coordinated complex of the magnesium cation with six water ( $\Theta$  mode).<sup>17</sup> The identical coordination geometry and very similar ion radius<sup>52</sup> of solvated  $\text{Ni}^{2+}$  compared to  $\text{Mg}^{2+}$  allow us to directly investigate if there are interactions *beyond* a pure confinement effect that influence the rattling frequency. Confinement being the dominant factor, the  $\text{Ni}^{2+}$  rattling frequency is given by  $\tilde{\nu}_{\text{Ni}^{2+}} \approx \sqrt{\frac{\mu_{\text{Mg}^{2+}(\text{aq})}}{\mu_{\text{Ni}^{2+}(\text{aq})}}} \tilde{\nu}_{\text{Mg}^{2+}}$  with  $\mu$  being the reduced mass of the mode in the solvated ion complex. Using the mode geometry described above, the reduced masses for  $\text{Mg}^{2+}(\text{aq})$  and  $\text{Ni}^{2+}(\text{aq})$  are 0.0328 and 0.0409 kg/mol, respectively. This yields a predicted center frequency of  $\tilde{\nu}_{\text{Ni}^{2+}} \approx 166 \text{ cm}^{-1}$  very close to our observed value of  $165 \text{ cm}^{-1}$ . The effective force constant for this mode is obtained from  $k = (2\pi\nu)^2 \times \mu$  and yields  $k = 65 \text{ N/m}$  for both magnesium and nickel. Assuming the same solvation geometry for  $\text{Mn}^{2+}(\text{aq})$  yields a reduced mass of 0.0402 kg/mol and a force constant of  $k = 44 \text{ N/m}$  for this mode, about two third of the value for  $\text{Ni}^{2+}$ .

In contrast to  $\text{Ni}^{2+}(\text{aq})$ ,  $\text{Mn}^{2+}(\text{aq})$  shows a cooperative effect influencing the *intensity*, not the center frequency of the second mode at  $214 \text{ cm}^{-1}$ . The intensity weakens with  $\text{Br}^-$  as counter anion compared to  $\text{Cl}^-$ .

## 4.2 Hydration water:

Figure 5 shows in the bottom left panel the influence of the different electrolytes on the surrounding solvation water. We are not able to determine the influences of anions and cations separately, however, the difference spectra put strong limitations on any choice of values: First, the cation difference spectra (see Figure 3, bottom) can be well described as difference of the  $\text{Mn}^{2+}$  damped harmonic modes minus those of  $\text{Ni}^{2+}$ , so that the influence of both cations on their solvation environment must be similar. Second, the same holds for the low frequency part ( $30\text{--}250 \text{ cm}^{-1}$ ) of the anion difference spectra. Considering the cooperative intensity change observed for both anions and cations, the negative difference in the frequency region  $250\text{--}350 \text{ cm}^{-1}$  of Figure 3, bottom left) is most likely due to a stronger effect of  $\text{Br}^-$  on the librational water band intensity compared to  $\text{Cl}^-$ . In our refined model we therefore attribute this negative deviation to  $\text{Br}^-$  instead of water in the vicinity of  $\text{Cl}^-$  as in Sharma et al.<sup>44</sup> Third, we observe negative  $\epsilon_{\text{ion}}^{\text{eff}}$  around  $200 \text{ cm}^{-1}$  which indicates that some water molecules absorb less than bulk water. We fit this with an effective parameter  $n_{\text{hydration}}$  that provides an estimate of the minimum number of water molecules that are influenced in the vicinity of solvated ions. THz absorption spectroscopy probes the collective and correlated hydrogen bond dynamics in the sub-picosecond range.<sup>42,53</sup> Thus, the dynamical hydration shell mentioned here differs from the concept of coordination spheres, which are generally described as the spatial

distribution of fixed water molecules around ions as well as the number of irrotationally bound water molecules observed in dielectric spectroscopy.<sup>54</sup> Within our measurement uncertainty  $n_{\text{hydration}} = 14.5$  was sufficient to describe the extinction deficiency for all four electrolytes investigated. This number is close to the sum  $n_{\text{hydration}} = 18$  of water molecules in the first solvation shell of one cation and two anions. According to reviews by Ohtaki and Radnai<sup>7</sup> and Buchner and Hefter<sup>54</sup> all four ions investigated here show approximately six water molecules in their first solvation shells.

The similarity of the water resonance observed in all four electrolytes may be interpreted in terms of a red-shifted hindered translational motion in the vicinity of the ions. Alternatively, symmetry-breaking in the coordination sphere of the first shell solvation water might lead to IR activity of the otherwise IR inactive mode of bulk water around  $150 \text{ cm}^{-1}$  as found in ab initio MD simulations.<sup>53</sup>

The solvation water spectrum obtained according to our model is not much influenced by the type of cation. While for frequencies below  $100 \text{ cm}^{-1}$  the extinction coefficients for the transition metal chlorides are very similar to those of bulk water, this changes in the high frequency end, where we find an increased extinction. Compared to the chlorides, the bromides show enhanced extinction coefficients over the full frequency range observed. Additional experimental and theoretical efforts will have to be undertaken to understand this behavior.

There is an ongoing discussion up to which extent ligand field stabilization affects the hydration dynamics of transition metal ions in aqueous phase.<sup>19,21,22</sup> In the dilute solution regime, it has been previously reported that at divalent charge state the  $\text{Mn}^{2+}(\text{d}5)$  hydrated ions have no additional ligand field stabilization effects due to their half occupied d-orbital.<sup>21,22</sup> In contrast,  $\text{Ni}^{2+}$  with its (d8) configuration shows strong ligand field stabilization effects.<sup>21,22</sup> Aakesson et. al.<sup>21</sup> have determined hydration enthalpy ( $\Delta H_{\text{hydration}}$ ), binding energy ( $\Delta E_{\text{binding}}$ ) and solvation energy ( $\Delta E_{\text{solvation}}$ ) of the divalent 3d-transition metal ions in gas and solution phases using ab initio methods. Their results indicate that, in dilute solution regime,  $\text{Mn}^{2+}$  does not have any additional ligand field stabilization effects, while these effects are clearly present in case of  $\text{Ni}^{2+}$ . This statement is supported by the larger cation–water distance for  $\text{Mn}^{2+}$  compared to  $\text{Ni}^{2+}$ .<sup>52</sup> From our data we find no evidence of ligand field stabilization effects on the dynamical solvation shell size of  $\text{Ni}^{2+}$  compared to  $\text{Mn}^{2+}$  beyond larger confinement.

## 4.3 Ion Pairing

With known effective molar extinctions of anions and cations, the extinction of ion pairs is given by  $\epsilon_{\text{pair}}^{\text{eff}} = \epsilon_{\text{diff}}^{\text{eff}} + \epsilon_{\text{cation}}^{\text{eff}} + \epsilon_{\text{anion}}^{\text{eff}}$  (see Equation (4)). By assuming that the effects of the individual ions on their solvation environment ( $n_{\text{hydration}}$ ,  $n_{\text{LF}}$ ,

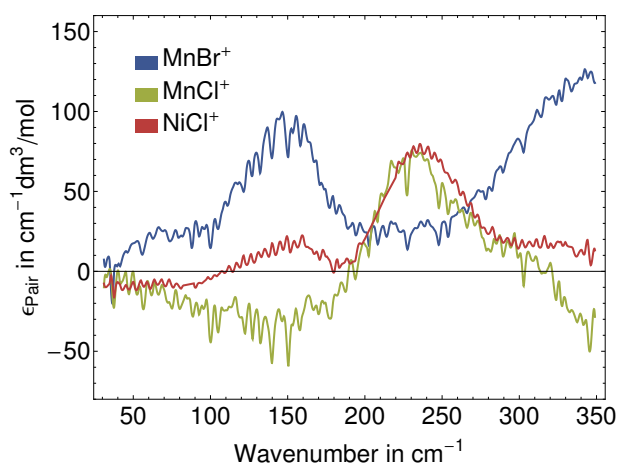


**Fig. 6** Molar extinction coefficients of different ion pairs in the THz/FIR frequency range assuming solvation water changes that are similar for all ions.

$n_{\text{HF}}$ , water low frequency mode in Table 2) are identical we are able to obtain approximate ion pair molar extinction coefficients (see Figure 6) and to get a qualitative picture of ion pairing effects.

$\text{MnCl}^+$  (green) shows a single strong resonance around  $230\text{ cm}^{-1}$  and a weak high frequency shoulder around  $300\text{ cm}^{-1}$ . We interpret the missing cation rattling mode around  $140\text{ cm}^{-1}$  as a strong indication of contact ion pair formation. This is in line with previous papers on  $\text{MnCl}_2$  which find that contact ion pairs are favored compared to solvent shared ion pairs: Libus and Tialowska<sup>55</sup> interpreted potentiometric and photometric measurements in terms of inner shell ( $\text{MnCl}(\text{H}_2\text{O})_5$ )<sup>+</sup> ion pairs and Waizumi et al.<sup>56</sup> observed mixed-ligand chloroaqua octahedral complexes in saturated aqueous  $\text{MnCl}_2$  solutions. Beagley et al.<sup>37</sup> and Un et al.<sup>39</sup> performed EXAFS measurements and electron paramagnetic resonance measurements, respectively, finding contact ion pairs.

$\text{MnBr}^+$  (blue) shows two strong resonances at  $150\text{ cm}^{-1}$ , and  $350\text{ cm}^{-1}$  and a weaker one at around  $80\text{ cm}^{-1}$ . The water resonance around  $185\text{ cm}^{-1}$  that was found for  $\text{LaBr}_3$  and interpreted as sign of solvent shared ion pair formation<sup>44</sup> is missing. Again, our finding supports ion pair formation in agreement with EXAFS data<sup>37</sup>, where an increased formation of inner shell ion pairs was found for  $\text{MnBr}^+$ .

$\text{NiCl}^+$  (red) contains spectral elements visible in both,  $\text{MnCl}^+$  and  $\text{MnBr}^+$ : the strongest resonance of  $\text{NiCl}^+$  (red) is centered around  $230\text{ cm}^{-1}$  and nearly identical to the main resonance found for  $\text{MnCl}^+$  (green). Secondly, when we use the  $\text{MnCl}^+$  (green) spectrum as reference, the weaker  $\text{NiCl}^+$  components resemble an attenuated version of the  $\text{MnBr}^+$  spectrum with similar line shapes for the band centered at  $150\text{ cm}^{-1}$  and enhanced extinction at  $80$  and  $350\text{ cm}^{-1}$ . This

finding is very surprising taking into account, that both anion and cation are different for  $\text{NiCl}^+$  and  $\text{MnBr}^+$  and indicates that the resonances common to  $\text{NiCl}^+$  and  $\text{MnBr}^+$  are due to water in the ion pair complex rather than anion-cation contact pair modes. Compared to  $\text{MnCl}_2$ , the literature data for  $\text{NiCl}_2$  are rather inconclusive. While neutron scattering data over a large concentration range<sup>27</sup> showed no evidence of contact ion pairs, NMR measurements<sup>25,26</sup> strongly favor the formation of contact ion pairs with one  $\text{Cl}^-$  in the cation hydration shell at concentrations close to the saturation limit. More recent data using EXAFS in combination with DFT and CPMD methods<sup>31</sup> claim no evidence for contact ion pairs. Aziz et al.<sup>30</sup> interpreted XANES measurements in terms of a continuous distortion effect for concentrations up to  $1.5\text{M}$ . The strong similarity of the main peak at  $230\text{ cm}^{-1}$  for both chlorides indicates that at least part of the  $\text{Ni}^{2+}$  cations form contact ion pairs with their counter ions in agreement with the NMR data.<sup>25,26</sup>

## 5 Summary and Conclusion

In conclusion, we have carried out high precision THz/FIR absorption measurements of  $\text{MnCl}_2$ ,  $\text{MnBr}_2$ ,  $\text{NiCl}_2$ , and  $\text{NiBr}_2$  in aqueous solution using  $30\text{--}350\text{ cm}^{-1}$  Fourier Transform spectroscopy in the concentration range  $0.5\text{--}4\text{ mol/dm}^3$ . The absorption spectra show a nonlinear concentration dependence, an indication of ion pair formation in concentrated solutions. Using a combination of principal component analysis and the chemical equilibrium model developed by us for lanthanide halides<sup>44</sup> allowed us to dissect the absorption spectra into effective ionic and ion pair contributions.

A global fit of the effective ionic extinction coefficients and their differences based on a properly chosen damped harmonic oscillator line function allowed us to derive individual anionic and cationic extinction coefficients and the combined effect of anions and cations on the solvation water spectrum. Within error bars, our experimental data are consistent with a physical interpretation where all anion and cation resonances are treated as Brownian harmonic oscillators that couple to the same set of thermal bath states. From the damping factor we obtain a decay  $\tau \approx 140\text{ fs}$  for the dipole moment autocorrelation function. The damping factor yields also an approximate limit between relaxational processes and oscillatory processes. Below a frequency  $\nu_d \ll \frac{\omega_0}{2\pi} = 37\text{ cm}^{-1}$  the oscillatory motion is masked by the exponential decay and the process may be considered as purely relaxational. As expected for the weakly solvated moieties the anion spectra consist of a single resonance attributed to the oscillatory Brownian motion of the anions with their solvation cage. The anion extinction differences for nickel and manganese halides are essentially identical to those reported before by us.<sup>17,44</sup> Both cations show more than one resonance indicating a strongly structured "su-

permolcular" solvation shell. The cation extinction spectra for  $\text{Mn}^{2+}(\text{aq})$  and  $\text{Ni}^{2+}(\text{aq})$  show a striking similarity: both contain two main peaks that are blueshifted in  $\text{Ni}^{2+}$  compared to  $\text{Mn}^{2+}$ . This can be interpreted in terms of a reduced confinement of solvated  $\text{Mn}^{2+}$  cations in aqueous solution compared to  $\text{Ni}^{2+}$ . We assign the main low-frequency resonances to the  $\Theta$  and  $\Psi$  IR-active normal modes of the octahedrally coordinated solvated cation complex reported by Funkner et al.<sup>17</sup>  $\text{Mn}^{2+}$  displays a third mode, that is possibly related to the symmetric  $\text{Mn}^{2+}\text{-O}$  stretch observed in Raman measurements. Both, anions and cations show a small cooperativity effect that influences the transition strengths. However, the center frequencies of the observed resonances remain unchanged.

The similar solvation shell size of the ions investigated, allowed us to extract a direct estimate of the combined effect of the ions on the spectra of water in their dynamical solvation shell. Within our measurement errors, we observe a THz defect in the frequency region of the hindered translational mode around  $200\text{ cm}^{-1}$  that is consistent with the total number eighteen of first shell solvation water for one cation and two anions in solution. At lower frequencies this deficiency is partly compensated by a water mode centered at  $133\text{ cm}^{-1}$  and the water relaxational term. At higher frequencies all salt solutions show an increased extinction compared to bulk water. In general, bromides show an increased molar extinction coefficient in the solvation water spectrum compared to chlorides.

From the single ion and solvation shell spectra we were able to obtain approximate ion pair extinction spectra for  $\text{MnCl}_2$ ,  $\text{MnBr}_2$ , and  $\text{NiCl}_2$ . All three electrolytes show indications of contact ion pair formation.

The work presented here demonstrates that concentration dependent THz and FIR absorption spectroscopy of electrolyte solutions provides valuable insight in structural and dynamical processes in aqueous solutions that is complementary to other spectroscopic techniques.

## 6 Appendix

The functional form of the water extinction coefficient as function of the frequency in wavenumber units at  $20^\circ\text{C}$  is given as a sum over a single relaxational term and three damped harmonic oscillator functions with a damping factor that depends exponentially on the frequency:

$$\begin{aligned} \varepsilon(\tilde{\nu}, 20^\circ\text{C}) &= \frac{a_0 \exp\left(-\frac{\tilde{\nu}}{\tilde{\nu}_0}\right)}{\pi \left(\tilde{\nu}^2 + \frac{\tilde{\nu}_0^2}{\pi^2}\right)} \tilde{\nu}^2 \\ &+ \sum_{i=1}^3 \frac{a_i \tilde{w}_i(\tilde{\nu})^2}{4\pi^3 \left(\left(\tilde{\nu}_i^2 + \frac{\tilde{w}_i(\tilde{\nu})^2}{4\pi^2} - \tilde{\nu}^2\right)^2 + \frac{\tilde{\nu}^2 \tilde{w}_i(\tilde{\nu})^2}{\pi^2}\right)} \tilde{\nu}^2 \end{aligned} \quad (9)$$

where  $\tilde{w}_i(\tilde{\nu}) = \tilde{w}_i(0) \exp\left(-\frac{\tilde{\nu}}{\tilde{\nu}_{\text{co},i}}\right)$  describes a frequency dependent damping factor with cutoff frequency  $\tilde{\nu}_{\text{co},i}$ . The parameters are given in Table 3.

i	$a_i$ in $\text{cm}^{-1} \text{ dm}^3/\text{mol}$	$\tilde{\nu}_0$ in $\text{cm}^{-1}$	$\tilde{w}_i(0)$ in $\text{cm}^{-1}$	$\tilde{\nu}_{\text{co},i}$ in $\text{cm}^{-1}$
0	14.36	–	53.93	520.86
1	183.49	157.03	789.34	520.86
2	152.54	437.9	8231.7	422.95
3	708.2	649.1	17261	322.68

**Table 3** Parametrization of the water extinction at  $20^\circ\text{C}$ . The absorption was determined using a conversion factor of  $55.41\text{ mol}/\text{dm}^3$  bulk water at this temperature.

It was obtained from a temperature dependent water measurement that was referenced to the etalon-corrected water data at  $25^\circ\text{C}$  from Bertie and Lan.<sup>45</sup> The estimated accuracy of the model is  $\pm 2\%$  over the frequency range  $30\text{--}400\text{ cm}^{-1}$ . A detailed discussion on the choice of selected line shapes is beyond the scope of this publication. The water absorption coefficient was obtained by multiplying Equation (9) by  $55.41$ , the number of mols of water in  $1\text{ dm}^3$  of the bulk liquid.

## Acknowledgement

We acknowledge E. Bründermann, E. Edengeiser, and H. Weingärtner for scientific support and helpful discussions. V.S. thankfully acknowledges financial support from the Ruhr-University Research School funded by Germany's Excellence Initiative [DFG GSC 98/1]. This work is supported by the Cluster of Excellence RESOLV (EXC1069) funded by the Deutsche Forschungsgemeinschaft.

## References

- 1 L. Deguillaume, M. Leriche, K. Desboeufs, G. Mailhot, C. George and N. Chaumerliac, *Chemical reviews*, 2005, **105**, 3388–3431.
- 2 J. B. Goodenough and Y. Kim, *Chemistry of Materials*, 2010, **22**, 587–603.
- 3 P. Jungwirth and D. J. Tobias, *Chemical Reviews*, 2006, **106**, 1259–1281.
- 4 H. Misonou, D. P. Mohapatra, E. W. Park, V. Leung, D. Zhen, K. Misonou, A. E. Anderson and J. S. Trimmer, *Nature neuroscience*, 2004, **7**, 711–718.
- 5 Y. Marcus and G. Hefter, *Chemical reviews*, 2006, **106**, 4585–4621.
- 6 G. Hefter, *Pure and applied chemistry*, 2006, **78**, 1571–1586.
- 7 H. Ohtaki and T. Radnai, *Chemical Reviews*, 1993, **93**, 1157–1204.
- 8 L. Helm and A. E. Merbach, *Chemical Reviews*, 2005, **105**, 1923–1960.
- 9 H. J. Bakker, *Chemical Reviews*, 2008, **108**, 1456–1473.
- 10 Y. Marcus, *Chemical Reviews*, 2009, **109**, 1346–1370.
- 11 I. Persson, *Pure and Applied Chemistry*, 2010, **82**, 1901–1917.
- 12 I. Heisler and S. Meech, *Science*, 2010, **327**, 857.
- 13 A. Omta, M. Kropman, S. Woutersen and H. Bakker, *Science*, 2003, **301**, 347.
- 14 W. Yellin and R. Plane, *Journal of the American Chemical Society*, 1961, **83**, 2448–2452.
- 15 D. Schmidt, O. Birer, S. Funkner, B. Born, R. Gnanasekaran, G. Schwaab, D. Leitner and M. Havenith, *Journal of the American Chemical Society*, 2009, **131**, 18512–18517.

- 16 K. Tielrooij, N. Garcia-Araez, M. Bonn and H. Bakker, *Science*, 2010, **328**, 1006.
- 17 S. Funkner, G. Niehues, D. A. Schmidt, M. Heyden, G. Schwaab, K. M. Callahan, D. J. Tobias and M. Havenith, *Journal of the American Chemical Society*, 2012, **134**, 1030–1035.
- 18 P. Jungwirth, *The Journal of Physical Chemistry B*, 2014.
- 19 P. Giaquinta, M. Tosi and N. March, *Physics and Chemistry of Liquids and International Journal*, 1983, **13**, 1–24.
- 20 J. E. Enderby, S. Cummings, G. J. Herdman, G. W. Neilson, P. S. Salmon and N. Skipper, *The Journal of Physical Chemistry*, 1987, **91**, 5851–5858.
- 21 R. Aakesson, L. Pettersson, M. Sandstroem and U. Wahlgren, *Journal of the American Chemical Society*, 1994, **116**, 8691–8704.
- 22 D. Johnson and P. Nelson, *J. Chem. Soc., Dalton Trans.*, 1995, 3483–3488.
- 23 H. Kanno, *The Journal of Physical Chemistry*, 1988, **92**, 4232–4236.
- 24 R. H. Stokes, S. Phang and R. Mills, *Journal of Solution Chemistry*, 1979, **8**, 489–500.
- 25 H. Weingärtner and H. G. Hertz, *J. Chem. Soc., Faraday Trans. 1*, 1979, **75**, 2700–2711.
- 26 H. Weingärtner, C. Müller and H. G. Hertz, *J. Chem. Soc., Faraday Trans. 1*, 1979, **75**, 2712–2734.
- 27 D. Powell and G. Neilson, *Journal of Physics: Condensed Matter*, 1990, **2**, 3871.
- 28 R. Caminiti and P. Cucca, *Chemical Physics Letters*, 1982, **89**, 110–114.
- 29 N. T. Skipper, G. W. Neilson and S. C. Cummings, *Journal of Physics: Condensed Matter*, 1989, **1**, 3489.
- 30 E. F. Aziz, S. Eisebitt, F. de Groot, J. W. Chiou, C. Dong, J. Guo and W. Eberhardt, *The Journal of Physical Chemistry B*, 2007, **111**, 4440–4445.
- 31 F.-F. Xia, D. Zeng, H.-B. Yi and C. Fang, *The Journal of Physical Chemistry A*, 2013, **117**, 8468–8476.
- 32 P. D'Angelo, O. M. Roscioni, G. Chillemi, S. Della Longa and M. Benfatto, *Journal of the American Chemical Society*, 2006, **128**, 1853–1858.
- 33 M. P. Fontana, G. Maisano, P. Migliardo and F. Wanderlingh, *The Journal of Chemical Physics*, 1978, **69**, 676–683.
- 34 Y. Inada, A. M. Mohammed, H. H. Loeffler and B. M. Rode, *The Journal of Physical Chemistry A*, 2002, **106**, 6783–6791.
- 35 M. Bustamante, I. Valencia and M. Castro, *The Journal of Physical Chemistry A*, 2011, **115**, 4115–4134.
- 36 J. Fryer and D. Morris, *Talanta*, 1968, **15**, 1309–1312.
- 37 B. Beagley, C. McAuliffe, S. Smith and E. White, *Journal of Physics: Condensed Matter*, 1991, **3**, 7919.
- 38 P.-A. Bergström and J. Lindgren, *Inorganic chemistry*, 1992, **31**, 1529–1533.
- 39 S. Un and A. Sedoud, *Applied Magnetic Resonance*, 2010, **37**, 247–256.
- 40 E. M. Gale, J. Zhu and P. Caravan, *Journal of the American Chemical Society*, 2013, **135**, 18600–18608.
- 41 S. Ebbinghaus, S. Kim, M. Heyden, X. Yu, M. Gruebele, D. Leitner and M. Havenith, *Journal of the American Chemical Society*, 2008, **130**, 2374–2375.
- 42 U. Heugen, G. Schwaab, E. Brndermann, M. Heyden, X. Yu, D. Leitner and M. Havenith, *Proceedings of the National Academy of Sciences*, 2006, **103**, 12301.
- 43 M. Heyden, E. Brndermann, U. Heugen, G. Niehues, D. Leitner and M. Havenith, *Journal of the American Chemical Society*, 2008, **130**, 5773–5779.
- 44 V. Sharma, F. Böhm, M. Seitz, G. Schwaab and M. Havenith, *Phys. Chem. Chem. Phys.*, 2013, **15**, 8383–8391.
- 45 J. E. Bertie and Z. Lan, *Appl. Spectrosc.*, 1996, **50**, 1047–1057.
- 46 H. R. Zelsmann, *Journal of Molecular Structure*, 1995, **350**, 95 – 114.
- 47 W. Press, B. P. Flannery, S. Teukolsky and W. T. Vetterling, *Numerical Recipes: The Art of Scientific Computing*, Cambridge University Press, Cambridge, 1986.
- 48 R. N. Goldberg, *Journal of Physical and Chemical Reference Data*, 1979, **8**, 1005–1050.
- 49 R. N. Goldberg, R. L. Nuttall and B. R. Staples, *Journal of Physical and Chemical Reference Data*, 1979, **8**, 923–1003.
- 50 T. Fukasawa, T. Sato, J. Watanabe, Y. Hama, W. Kunz and R. Buchner, *Phys. Rev. Lett.*, 2005, **95**, 197802.
- 51 A. Nitzan, *Chemical Dynamics in Condensed Phases: Relaxation, Transfer and Reactions in Condensed Molecular Systems: Relaxation, Transfer and Reactions in Condensed Molecular Systems*, Oxford University Press, 2006.
- 52 Y. Marcus, *Chemical Reviews*, 1988, **88**, 1475–1498.
- 53 M. Heyden, J. Sun, S. Funkner, G. Mathias, H. Forbert, M. Havenith and D. Marx, *Proceedings of the National Academy of Sciences*, 2010, **107**, 12068.
- 54 R. Buchner and G. Hefter, *Physical Chemistry Chemical Physics*, 2009, **11**, 8984–8999.
- 55 Z. Libuš and H. Tialowska, *Journal of Solution Chemistry*, 1975, **4**, 1011–1022.
- 56 K. Waizumi, T. Kouda, A. Tanio, N. Fukushima and H. Ohtaki, *Journal of Solution Chemistry*, 1999, **28**, 83–100.

Assignment	Parameter	MnCl <sub>2</sub>	MnBr <sub>2</sub>	NiCl <sub>2</sub>	NiBr <sub>2</sub>
hydration water	$n_{\text{hydration}}$	14.5(5)			
water relaxational mode	$n_{LF}$	16.4(5)	18.9(5)	MnCl <sub>2</sub>	MnBr <sub>2</sub>
water	$\tilde{\nu}_d$ in cm <sup>-1</sup>	113(2)			
low frequency mode	$\tilde{\nu}_0$ in cm <sup>-1</sup>	133(2)			
	$a$ in cm <sup>-1</sup> dm <sup>3</sup> /mol	553(46)			
	$w$ in cm <sup>-1</sup>	444(22), ( $\tau = 75$ fs)			
water libration	$n_{HF}$	19.9(5)	23.6(5)	MnCl <sub>2</sub>	22.9(5)
M <sup>2+</sup> (aq) Θ mode <sup>17</sup>	$\tilde{\nu}_d$ in cm <sup>-1</sup>	134.8(2)		160.5(3)	
	$\tilde{\nu}_0$ in cm <sup>-1</sup>	139.7(2)		164.7(3)	
	$a$ in cm <sup>-1</sup> dm <sup>3</sup> /mol	1598(28)		1545(29)	
	$w$ in cm <sup>-1</sup>	232(1), ( $\tau = 140$ fs)			
M <sup>2+</sup> (aq) Ψ mode <sup>17</sup>	$\tilde{\nu}_d$ in cm <sup>-1</sup>	214(1)		262(1)	
	$\tilde{\nu}_0$ in cm <sup>-1</sup>	217(1)		265(1)	
	$a$ in cm <sup>-1</sup> dm <sup>3</sup> /mol	548(121)	360(11)	211(5)	
	$w$ in cm <sup>-1</sup>	Θ mode			
M <sup>2+</sup> (aq) unknown	$\tilde{\nu}_d$ in cm <sup>-1</sup>	360(4)		–	
	$\tilde{\nu}_0$ in cm <sup>-1</sup>	362(4)		–	
	$a$ in cm <sup>-1</sup> dm <sup>3</sup> /mol	337(32)		–	
	$w$ in cm <sup>-1</sup>	Θ mode		–	
X <sup>-</sup> (aq) anion rattling <sup>17</sup>	$\tilde{\nu}_d$ in cm <sup>-1</sup>	183.7(2)	87(1)	MnCl <sub>2</sub>	MnBr <sub>2</sub>
	$\tilde{\nu}_0$ in cm <sup>-1</sup>	187.4(2)	94(1)	MnCl <sub>2</sub>	MnBr <sub>2</sub>
	$a$ in cm <sup>-1</sup> dm <sup>3</sup> /mol	1346 (10)	101(8)	1263(6)	191(7)
	$w$ in cm <sup>-1</sup>	Θ mode			

**Table 2** Center frequency  $\tilde{\nu}_d$ , corrected center frequency  $\tilde{\nu}_0$ , amplitude  $a$ , and linewidth  $w$  obtained from a global fit of the eight spectra displayed in Figure 3. We have used damped harmonic oscillator line shapes (see Equation (8)) for the ionic and water resonances and scaled bulk water relaxational and librational modes as models for the low frequency and high frequency components. In addition, a contribution  $n_{\text{hydration}}$  was added accounting for the hydration water. The numbers in brackets correspond to  $2\sigma$  statistical errors. Values spanning several columns as well as text labels indicate that the same fit parameter was used for a description of line parameters for different resonances.

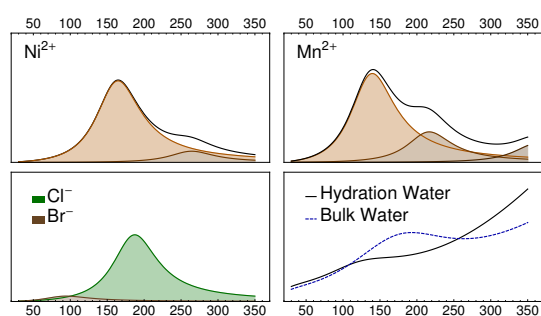


**Fig. 7** Table of content graphics: Concentration dependent THz/FIR absorption measurements allow determination of individual solvated ion resonances and their influence on the hydration water spectrum.